Communication in Physical Sciences, 2026, 13(2): 308-328

Enhanced Adsorptive Removal of Pb^{2+} and Cd^{2+} Ions from Aqueous Solution Using Phosphoric Acid–Activated Rice Husk

Magaji Ladan, Khadija Zubairu Muhammad and Shehu Habibu
Received: 02 January 2026/Accepted: 16 February 2026 /Published: 20 February 2026
https://dx.doi.org/10.4314/cps.v13i2.10

Abstract: *Adsorption is an efficient method for removing toxic metals from contaminated water, and this study investigates the performance of raw rice husk (RRH) and phosphoric acid–activated rice husk (ARH) for the removal of Pb(II) and Cd(II) ions from simulated aqueous solutions. The adsorbents were characterized using Fourier transform infrared spectroscopy (FTIR), Field emission scanning electron microscopy (FESEM), and Energy dispersive X-ray (EDX), confirming the presence of functional groups and porous surfaces suitable for adsorption. Batch experiments examined the effects of initial metal concentration (10–200 mg/L), contact time (0–60 min), solution pH (2–8), adsorbent dosage (0.5–3.0 g/L), and temperature (303–323 K). The optimum pH for Pb(II) adsorption was 4 for both RRH and ARH, while for Cd(II), the optimum pH was 5 on ARH and 7 on RRH. Adsorption equilibrium was achieved within 50 and 20 min for Pb(II), and 50 and 30 min for Cd(II) on ARH and RRH, respectively. Maximum adsorption capacities (q_m) determined from the Langmuir model were 133.33 mg/g for Pb(II) on ARH, 35.07 mg/g on RRH, 28.82 mg/g for Cd(II) on RRH, and 17.67 mg/g on ARH. Equilibrium data were best described by the Freundlich isotherm, with constants n ranging from 1.958 to 2.182, indicating favorable adsorption. Dubinin–Radushkevich analysis yielded mean free energies below 8 kJ/mol, confirming a physisorption-dominated mechanism. Kinetic studies followed the pseudo-second-order model, and thermodynamic parameters ($\Delta G°$ = –3.12 to –3.75 kJ/mol; $\Delta H°$ = –18.04 to –16.53 kJ/mol; $\Delta S°$ = +55.28 to +61.84 J/mol·K) indicated that the adsorption process is spontaneous and exothermic. These results demonstrate that rice husk and its activated form are effective, low-cost, and sustainable adsorbents for heavy metal remediation in aqueous environments.*

Keywords: *Rice husk; Heavy metals; Adsorption; Lead; Cadmium; Wastewater treatment*

Magaji Ladan
Department of Pure and Industrial Chemistry, Bayero University, Kano, Nigeria
Email: mladan.chm@buk.edu.ng
https://orcid.org/0000-0002-5602-6483

Khadija Zubairu Muhammad
Department of Pure and Industrial Chemistry, Bayero University, Kano, Nigeria
Email: khadijazubairumuhammad@gmail.com

Shehu Habibu
Department of Pure and Industrial Chemistry, Bayero University, Kano, Nigeria
Email: shabibu.chm@buk.edu.ng

1.0 Introduction

Heavy metal contamination of water resources has become a critical global environmental and public health challenge driven by rapid industrialization, urban expansion, mining activities, and intensified agricultural practices (Awaka-Ama *et al*., 2024). Heavy metals are characterized by high density and persistence in the environment, and they pose serious risks because they are non-biodegradable and capable of bioaccumulation in living organisms (Zhao *et al*., 2023). Elevated concentrations of toxic metal ions in soil and aquatic environments have been associated with ecological degradation, alteration of soil properties, and severe health disorders in

humans and animals (Naiya *et al*., 2009; Raikar *et al*., 2015). Numerous studies have reported the frequent detection of Pb^{2+} and Cd^{2+} ions in industrial effluents originating from battery manufacturing, electroplating, pigment production, and mining operations (Okwunodulu & Eddy, 2014; Eddy *et al*., 2024a)

Among various heavy metals, lead (Pb) and cadmium (Cd) are particularly hazardous owing to their high toxicity, mobility, and long biological half-lives. Exposure to Pb^{2+} and Cd^{2+} ions beyond permissible limits may occur through contaminated drinking water, inhalation of polluted air, or ingestion via the food chain, resulting in neurological damage, renal dysfunction, and carcinogenic effects (Asuquo & Martin, 2016; Hua *et al*., 2012). The widespread use of heavy metals in industrial processes has significantly increased their availability in natural water bodies, especially in developing regions where wastewater treatment infrastructure is often inadequate (Khashan & Mohammad, 2022; Prapagdee *et al*., 2016).

Several physicochemical techniques, including chemical precipitation, membrane filtration, coagulation, ion exchange, and electrochemical treatment, have been employed for the removal of heavy metals from wastewater (Ladan *et al*., 2024). Despite their effectiveness, these methods are often limited by high operational and capital costs, energy intensiveness, production of large volumes of toxic sludge, and the need for skilled manpower. Consequently, the development of cost-effective, efficient, and environmentally sustainable treatment technologies remains a critical research priority. While these conventional technologies can achieve high removal efficiencies, their large-scale application is often constrained by economic and operational challenges, particularly in developing countries where treatment infrastructure and technical expertise may be limited (Akpanudo & Chibuzo, 2020; Eddy *et al*., 2024b)

Adsorption has gained considerable attention as a promising alternative for wastewater remediation due to its simplicity, high removal efficiency, operational flexibility, and minimal sludge generation (Habibu *et al*., 2023). Agricultural wastes have attracted increasing interest as potential adsorbents due to their abundance, low cost, biodegradability, and rich surface chemistry. Among these materials, rice husk is a particularly attractive candidate because of its widespread availability and favorable chemical composition (Luo *et al*., 2019; Raikar *et al*., 2015). Previous investigations have explored various lignocellulosic materials such as coconut shells, sawdust, maize cob, and rice husk for heavy metal adsorption, demonstrating promising removal efficiencies depending on surface modification and operational conditions. Chemical activation can further enhance its adsorption capacity by increasing porosity and surface functional groups (Raikar *et al*., 2015).

Despite extensive research on agricultural waste–based adsorbents, comparative studies evaluating the adsorption performance of raw and phosphoric acid–activated rice husk for the simultaneous removal of Pb(II) and Cd(II) ions under systematically controlled conditions remain limited. In addition, comprehensive understanding of the adsorption mechanisms through combined kinetic, equilibrium, and thermodynamic analyses is still insufficient. Therefore, this study systematically investigates the adsorption behavior of Pb(II) and Cd(II) ions using raw rice husk (RRH) and phosphoric acid–activated rice husk (ARH) as low-cost and environmentally sustainable adsorbents through detailed characterization and batch adsorption analyses. The findings of this research are expected to contribute to the development of sustainable and economically viable wastewater treatment technologies, promote waste-to-resource valorization, and

provide insight into the practical application of agricultural biomass–derived adsorbents for heavy metal remediation, particularly in resource-limited regions.

2.0 Materials and Methods

2.1 Materials

All chemicals used in this study were of analytical reagent (AR) grade and were used as received without further purification. Lead nitrate ($Pb(NO_3)_2$, 99 %), cadmium sulphate octahydrate ($CdSO_4 \cdot 8H_2O$, 99 %), hydrochloric acid (HCl, 36.5 %), sodium hydroxide (NaOH, 99.8 %), phosphoric acid (H_3PO_4, 85 %), and nitric acid (HNO_3, 68 %) were employed for solution preparation, pH adjustment, and adsorbent activation. Deionized water was used throughout all experimental procedures.

2.2 Preparation of Raw Rice Husk (RRH)

Rice husk was collected from a local rice mill in Kura Local Government Area, Kano State, Nigeria. The material was manually cleaned to remove foreign particles and repeatedly washed with deionized water. The cleaned rice husk was oven dried at 80 °C for 24 h, ground into fine powder and sieved to obtain a uniform particle size (<250 µm), then stored in airtight containers for subsequent use. The prepared sample was designated as raw rice husk (RRH).

2.3 Preparation of Activated Rice Husk (ARH)

Activated rice husk was prepared following a modified procedure reported by (Alam *et al*., 2020; Korobochkin *et al*., 2016). The dried rice husk powder was first carbonized in a muffle furnace at 450 °C for 1.5 h under a closed system to obtain carbonized rice husk (CRH). The CRH was then chemically impregnated with 50 % (w/w) phosphoric acid at an impregnation ratio of 1:1 (CRH:H_3PO_4) and soaked for 24 h. The impregnated material was filtered and oven-dried at 105 °C overnight, followed by activation at 550 °C for 1.5 h. After cooling to room temperature, the activated product was washed with 1.0 M NaOH and repeatedly rinsed with hot and cold deionized water until neutral pH was attained. The final activated rice husk (ARH) was dried at 105 °C for 24 h, crushed, and stored in airtight containers.

2.4 Characterization of Adsorbents

Fourier transform infrared (FTIR) spectra were recorded using a Cary 630 FTIR spectrophotometer (Agilent Technologies). Surface morphology and elemental composition were analyzed using a scanning electron microscope equipped with energy dispersive X-ray spectroscopy (SEM–EDX, Philips XL 30). Residual metal ion concentrations were determined using an atomic absorption spectrometer (AAS, Varian T60, Agilent Technologies). A Jenway 3320 pH meter was used for pH measurements, while an analytical balance (FA 2004), muffle furnace (SXL 1008), and orbital shaker (Innova 4000, New Brunswick) were used during sample preparation and batch adsorption experiments.

2.5 Preparation of Metal Ion Solutions

Stock solutions (1000 mg L^{-1}) of Pb(II) and Cd(II) ions were prepared by dissolving appropriate amounts of $Pb(NO_3)_2$ and $CdSO_4 \cdot 8H_2O$, respectively, in deionized water. Working solutions of desired concentrations were prepared by serial dilution. Solution pH was adjusted using 0.1 M HCl or 0.1 M NaOH.

2.6 Batch Adsorption Experiments

Batch adsorption studies were conducted to evaluate the effects of initial metal ion concentration, contact time, solution pH, adsorbent dosage, and temperature, following modified procedures reported in the literature (Goel *et al*., 2005; Sazali *et al*., 2020). Typically, a known mass of adsorbent was added to 50 mL of metal ion solution in a 250 mL Erlenmeyer flask and agitated at 160 rpm on an orbital shaker. After the desired contact time, the suspensions were filtered using Whatman No. 41 filter paper, and the filtrates were analyzed using AAS. All experiments were performed in replicate, and average values were reported.

The percentage removal and equilibrium adsorption capacity (q_e, mg g^{-1}) were calculated using equation 1 (Akpanudo & Olabemiwo, 2024a,b; Ogoko *et al*., 2023).

$$\%Removal = \frac{C_0 - C_e}{C_0} \times \frac{100}{1} \quad (1)$$

where C_0 and C_e are the initial and final concentrations of metal ions in the solution.

2.7 Effect of Operational Parameters

The effect of initial metal ion concentration was investigated by varying Pb(II) and Cd(II) concentrations while maintaining constant adsorbent dosage and contact time. Contact time studies were carried out by varying agitation time at fixed initial concentration. Temperature effects were examined by conducting experiments at different temperatures under identical conditions. The influence of solution pH was evaluated over a selected pH range, while adsorbent dosage studies were performed by varying adsorbent mass at constant metal ion concentration.

3.0 Results and Discussion

3.1 Fourier transform infrared spectroscopy (FTIR)

The FTIR spectra of raw rice husk (RRH) and activated rice husk (ARH) before and after adsorption of Cd^{2+} and Pb^{2+} ions are presented in Figs. 1 and 2. The spectra reveal multiple characteristic peaks, reflecting the chemical complexity and heterogeneous surface nature of rice husk adsorbents, which is favorable for metal ion adsorption.

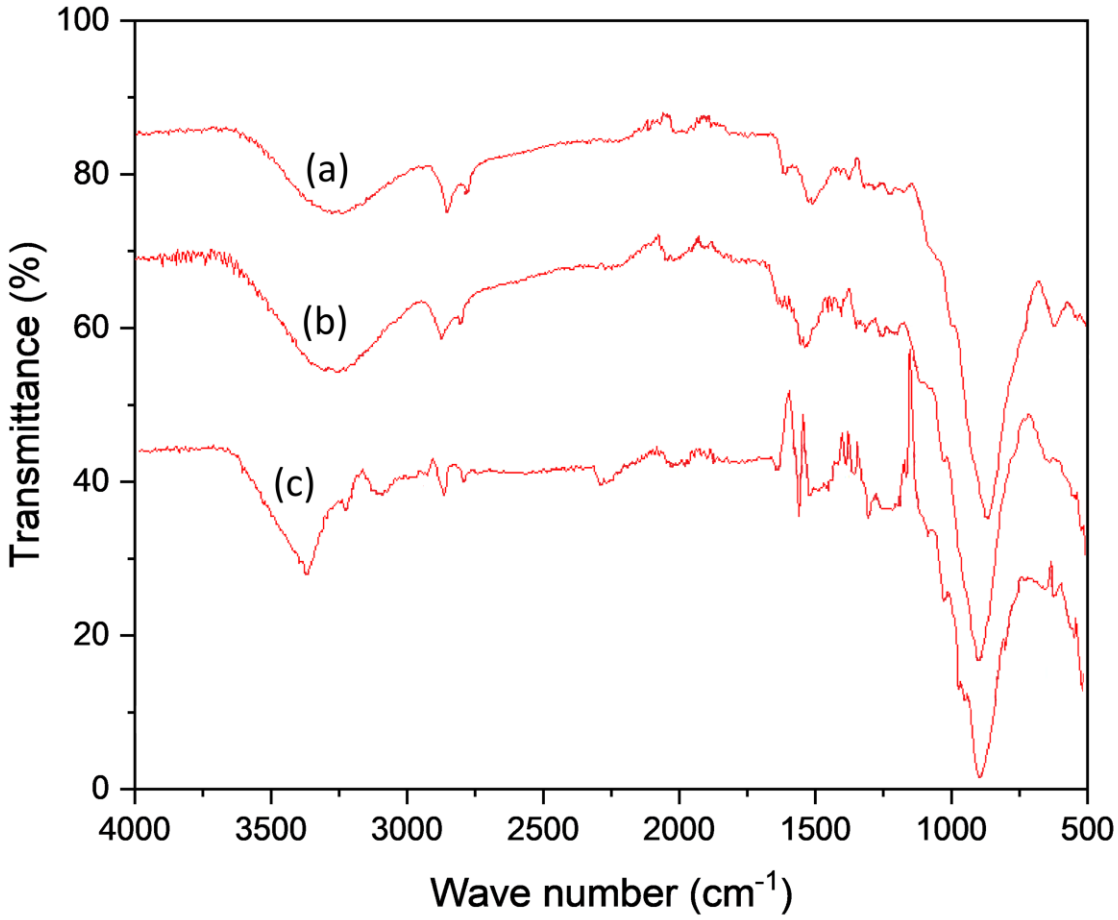

Fig. 1: FTIR Spectrum of (a) RRH before adsorption, (b) RRH after adsorption of Cd^{2+} ion and (c) RRH after adsorption of Pb^{2+}

A broad absorption band observed in the range of 3200–3550 cm^{-1} for RRH and ARH in Figs. 1a and 2a, respectively, is attributed to the stretching vibrations of bonded hydroxyl (–OH) groups, originating mainly from cellulose, hemicellulose, and lignin constituents. These hydroxyl groups are known to play a critical role in metal ion binding through hydrogen bonding and surface complexation mechanisms.

The absorption bands appearing between 2850 and 3000 cm^{-1} in the spectra of RRH before and after adsorption, shown in Figure 1 (a, b, and c) correspond to aliphatic C–H stretching vibrations, indicating the presence of alkyl groups within the biomass structure. The presence of carbonyl and carboxylic functional groups is confirmed by the peaks in the range of 1735–1750 cm^{-1}, attributed to C=O stretching vibrations, particularly evident in Figure 1 (a, b and c). These groups are widely reported as effective metal-binding sites due to their ability to form coordination bonds with divalent metal ions.

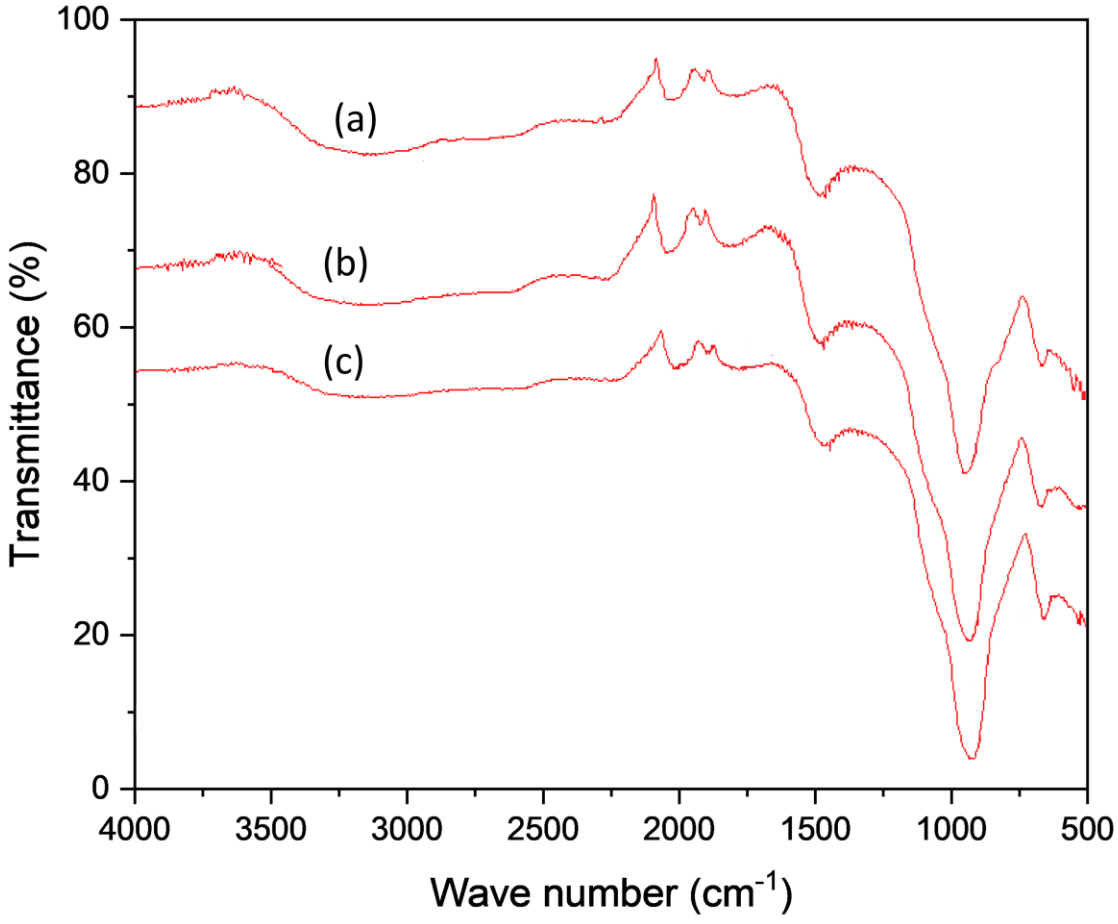

Fig. 2: FTIR spectrum of (a) ARH before adsorption, (b) ARH after adsorption of Cd^{2+} ion and (c) ARH after adsorption of Pb^{2+} ion

Aromatic C=C stretching vibrations were observed in the region 1640–1680 cm^{-1} indicated in Figure 2 (a, b and c), suggesting the presence of aromatic structures associated with lignin components. Additionally, the prominent bands between 1022 and 1063 cm^{-1}, present in all spectra (Figs 1 and 2), are assigned to C–O stretching vibrations, characteristic of alcohols, ethers, and polysaccharide structures. These functional groups further contribute to adsorption through

electrostatic interactions and surface complexation.

Upon activation of rice husk (RRH to ARH), noticeable shifts in peak positions were observed, particularly in the C–O stretching region from approximately 1030 cm^{-1} to 1063 cm^{-1} (Figures 1a and 2a). This shift toward higher wavenumbers indicates structural modification and enhanced surface reactivity due to the activation process. Furthermore, after the adsorption of Cd^{2+} and Pb^{2+} ions, a reduction in the intensity and, in some cases, partial disappearance of specific peaks, especially those around 1514, 1737, and 3201 cm^{-1} was observed. These changes provide strong evidence of interaction between metal ions and surface functional groups.

The observed peak shifts and intensity reductions suggest that adsorption occurred mainly through chemical interactions involving hydroxyl, carbonyl, and carboxyl functional groups. In particular, the dissociation of hydroxyl groups likely generates negatively charged surface sites that facilitate electrostatic attraction and complexation with Cd^{2+} and Pb^{2+} ions. Similar observations have been reported in previous studies, where changes in FTIR spectra after adsorption were attributed to successful metal binding on biomass-derived adsorbents.

Overall, the FTIR analysis confirms that both RRH and ARH possess abundant surface functional groups capable of interacting with heavy metal ions, while activation enhances surface functionality and adsorption efficiency. The spectral changes after adsorption clearly demonstrate that Cd^{2+} and Pb^{2+} removal is governed by surface complexation and chemical binding mechanisms rather than simple physical adsorption. The surface complexation of lead (Pb^{2+}) and cadmium (Cd^{2+}) ions with hydroxyl and carboxyl groups can be described by the following equilibrium equation:

$$C - OH + M^{2+} = C - O - M^{+} + H^{+} \quad (2)$$

where M^{2+} represents the divalent metal cation, $C - OH$ represents the reactive surface hydroxyl groups bound to the adsorbent matrix and $C - O - M^{+}$, the resulting surface-bound metal complex. This chemical interaction is a primary mechanism for heavy metal adsorption, where the metal ions displace hydrogen protons to form stable coordinative bonds with the oxygen atoms on the adsorbent's surface.

3.2 Scanning Electron Microscopy (SEM)

The SEM micrographs of raw rice husk (RRH) and activated rice husk (ARH) are presented in Fig. 3. Figs. 3a and 3b show the surface morphology of RRH and ARH before adsorption. Both adsorbents exhibit heterogeneous surfaces with irregular structures and well-developed pores, indicating high surface area and potential sites for metal ion adsorption. The activation process (ARH) appears to increase pore size and surface roughness, consistent with the enhanced accessibility of adsorption sites observed in the FTIR analysis, where activation introduced additional functional groups such as C–O and hydroxyl moieties.

Following adsorption of Pb^{2+} and Cd^{2+} ions (Figs. 3c–f), significant morphological changes are evident. The surfaces of both RRH and ARH became smoother, with visible pore blockage and partial collapse of the irregular features. For RRH (Figs. 3c and 3d), the accumulation of Pb^{2+} and Cd^{2+} ions is apparent in the reduced surface roughness and occlusion of pores. In ARH (Figs. 3e and 3f), the adsorption of metal ions is more pronounced, likely due to the increased number of active sites generated during phosphoric acid activation. These observations align with the FTIR results, which showed shifts and intensity reductions in peaks corresponding to hydroxyl, carbonyl, and carboxyl groups, confirming chemical interactions and surface complexation between the metal ions and functional groups on the adsorbents.

The SEM images corroborate the proposed adsorption mechanism: metal ions interact with both the physical pore structure and chemical surface sites of the adsorbents. The combination of enhanced porosity (physical adsorption) and the abundance of reactive surface functional groups (chemical adsorption) explains the higher adsorption efficiency of ARH compared to RRH, as observed in the batch adsorption experiments. Overall, the SEM analysis demonstrates that adsorption of Pb^{2+} and Cd^{2+} ions is accompanied by morphological alterations that are consistent with FTIR evidence of chemical bonding, highlighting the synergistic contribution of surface morphology and functional groups to the removal process.

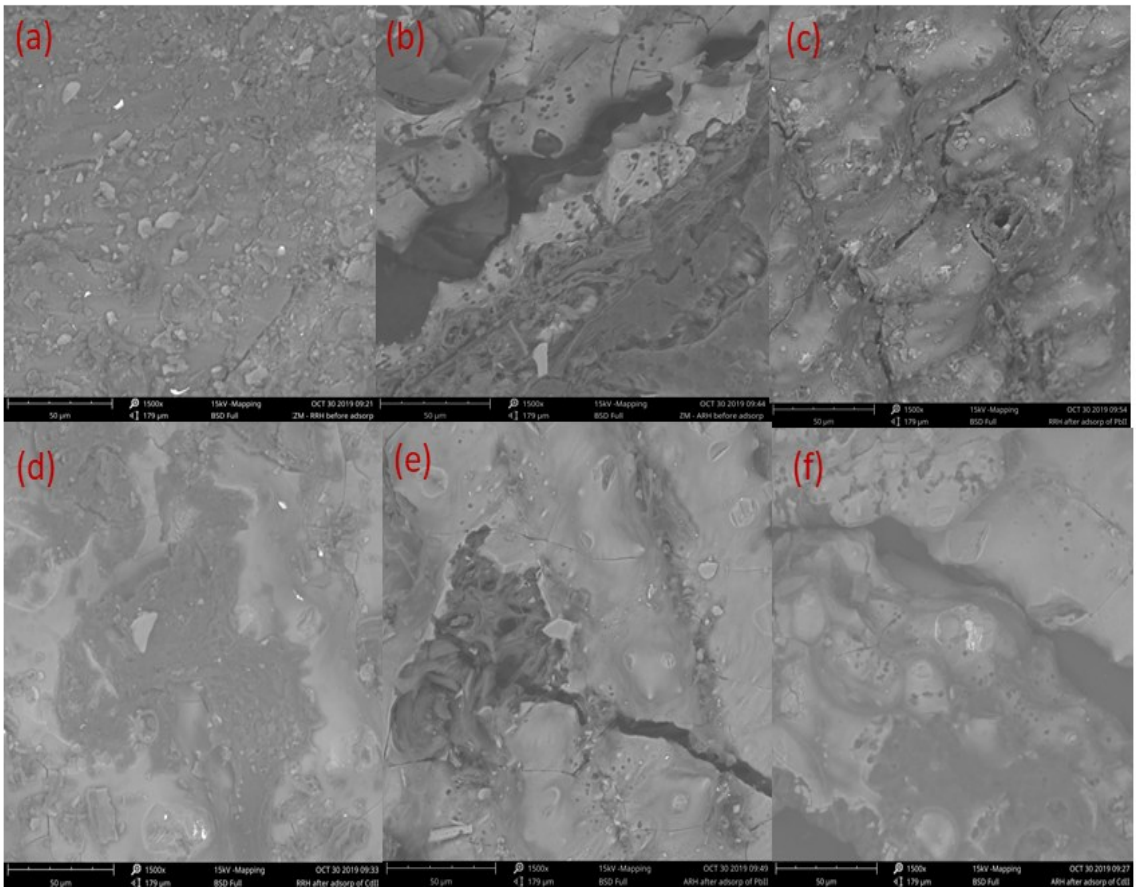

Fig. 3: SEM micrographs of (a) RRH before adsorption, (b) ARH before adsorption, (c) RRH after adsorption of Pb^{+2} ion, (d) RRH after adsorption of Cd^{+2} ion, (e) ARH after Adsorption of Pb^{+2} ion and (f) ARH after adsorption of Cd^{+2} ion

3.3 Effect of Initial Metal Ion Concentration

Fig. 4 illustrates the effect of initial Pb^{2+} and Cd^{2+} concentrations on adsorption by RRH and ARH. Adsorption capacity decreased with increasing initial concentration, with maximum uptake observed at 10 mg L^{-1} for both metal ions. This behavior reflects progressive saturation of a finite number of active adsorption sites at higher metal ion concentrations, leading to reduced adsorption efficiency. Similar concentration-dependent trends have been reported for Pb^{2+} and Cd^{2+} removal using modified *Spirulina platensis* and *Chlorella vulgaris* adsorbents (Muhammad *et al*., 2020; Pooladi *et al*., 2024) and other biosorbent systems (El-Bindary *et al*., 2015).

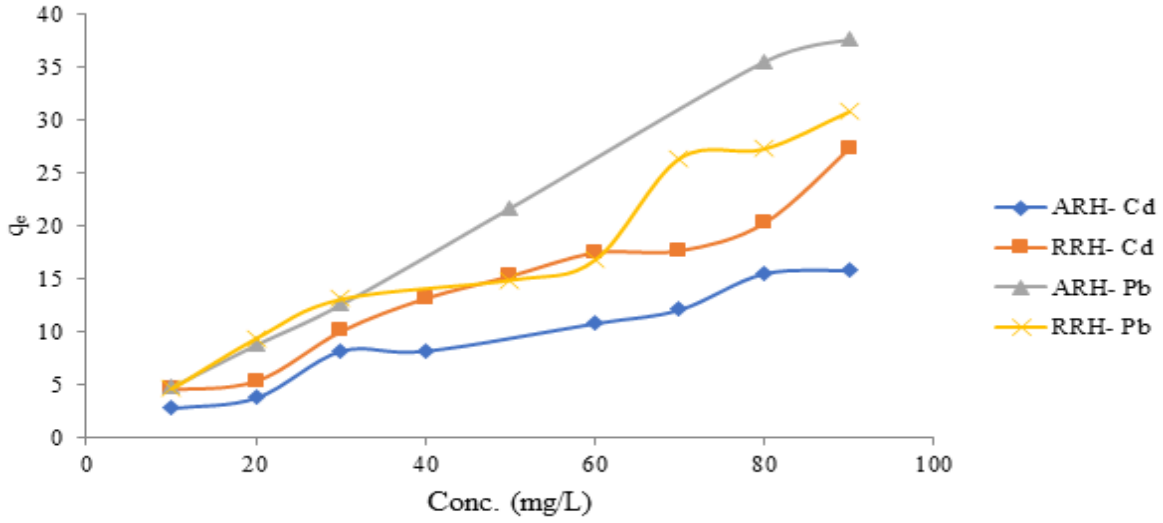

Fig. 4: Effect of initial concentration for removal of Cd^{2+} and Pb^{2+} ions onto RRH and ARH

3.4 Effect of Contact Time

The adsorption kinetics of Pb^{2+} and Cd^{2+} onto RRH and ARH are shown in Fig. 5. Rapid metal uptake occurred during the initial contact period, followed by a gradual approach to equilibrium, consistent with surface site saturation. Equilibrium was attained for Cd^{2+} at 50 and 30 min on ARH and RRH, respectively, while Pb^{2+} reached equilibrium at 50 and 20 min on ARH and RRH, respectively. The fast initial adsorption suggests a strong affinity between the metal ions and available active sites. Comparable equilibrium behavior has been reported for Pb^{2+} and Cd^{2+} adsorption on γ-Al_2O_3 nanoparticles (Jalu *et al*., 2025).

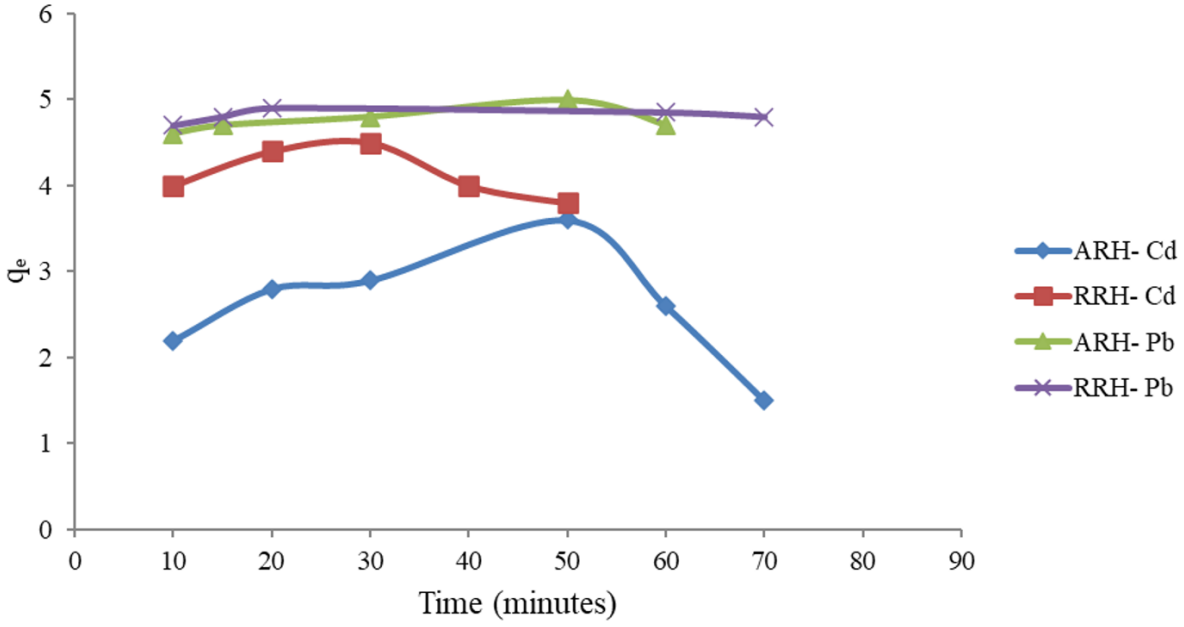

Fig. 5: Effect of contact time for the removal of Cd^{2+} and Pb^{2+} ions onto RRH and ARH

3.5 Effect of Temperature

The effect of temperature on Pb^{2+} and Cd^{2+} adsorption is presented in Fig. 6. Adsorption capacity generally decreased with increasing temperature, indicating an exothermic adsorption process. Elevated temperatures likely weaken electrostatic interactions and enhance desorption of metal ions from the adsorbent surface. Similar temperature-dependent decreases in adsorption capacity have been observed for Cd^{2+} adsorption using *Ulva lactuca* and for Pb^{2+} removal using biomass-derived adsorbents (Ali *et al*., 2024; Babu *et al*., 2018; thi Quyen *et al*., 2021). These findings are consistent with thermally induced disruption of adsorbate–adsorbent interactions (Ali *et al*., 2024).

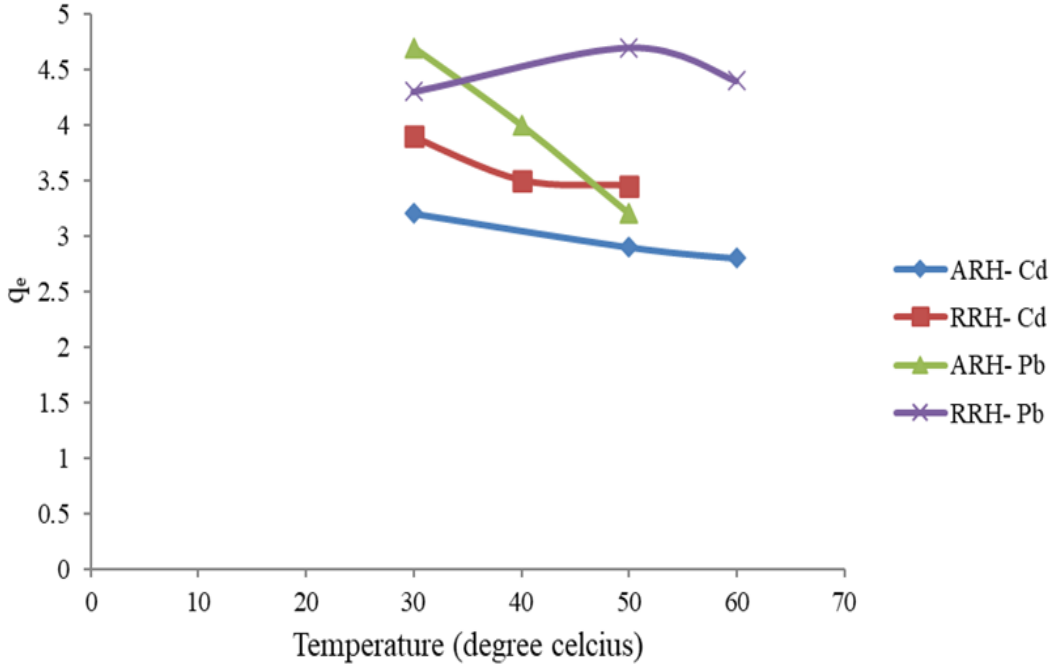

Fig. 6: Effect of temperature for the removal of Pb^{2+} and Cd^{2+} ions onto ARH and RRH adsorbent

3.6 Effect of Solution pH

Solution pH significantly influenced Pb^{2+} and Cd^{2+} adsorption due to its effect on adsorbent surface charge and metal ion speciation (Fig. 7). Adsorption increased from pH 3 to 4, reaching optimum values at pH 5 (ARH) and pH 7 (RRH) for Cd^{2+}, while maximum Pb^{2+} adsorption occurred at pH 4 for both adsorbents. Reduced adsorption at low pH is attributed to competition between protons and metal ions for active sites, whereas decreased uptake at higher pH may result from metal hydroxide formation or electrostatic repulsion. Similar pH-dependent adsorption behavior has been widely reported for Pb^{2+} and Cd^{2+} using biomass-derived and nanostructured adsorbents (Moyo *et al*., 2013; Raiker *et al*., 2015; Asuquo and Martin, 2016; Tabesh *et al*., 2017; Huang and Keller, 2015).

3.7 Effect of Adsorbent Dosage

Fig. 8 shows the influence of adsorbent dosage on Pb^{2+} and Cd^{2+} adsorption. Increasing adsorbent mass enhanced adsorption capacity due to increased availability of active sites, up to an optimum dosage beyond which no significant improvement was observed, likely due to site saturation and particle aggregation. Optimum dosages of 0.6 g for ARH and RRH yielded Cd^{2+} adsorption capacities of 0.63 and 0.79 mg g^{-1}, respectively. For Pb^{2+}, optimum dosages of 0.5 g (ARH) and 0.6 g (RRH)

resulted in adsorption capacities of 0.85 and 0.79 mg g^{-1}, respectively. These results align with previous reports on Pb^{2+} and Cd^{2+} adsorption using agricultural and algae-based adsorbents (Gaya *et al*., 2015; Sayadi *et al*., 2019; Tabesh *et al*., 2017)

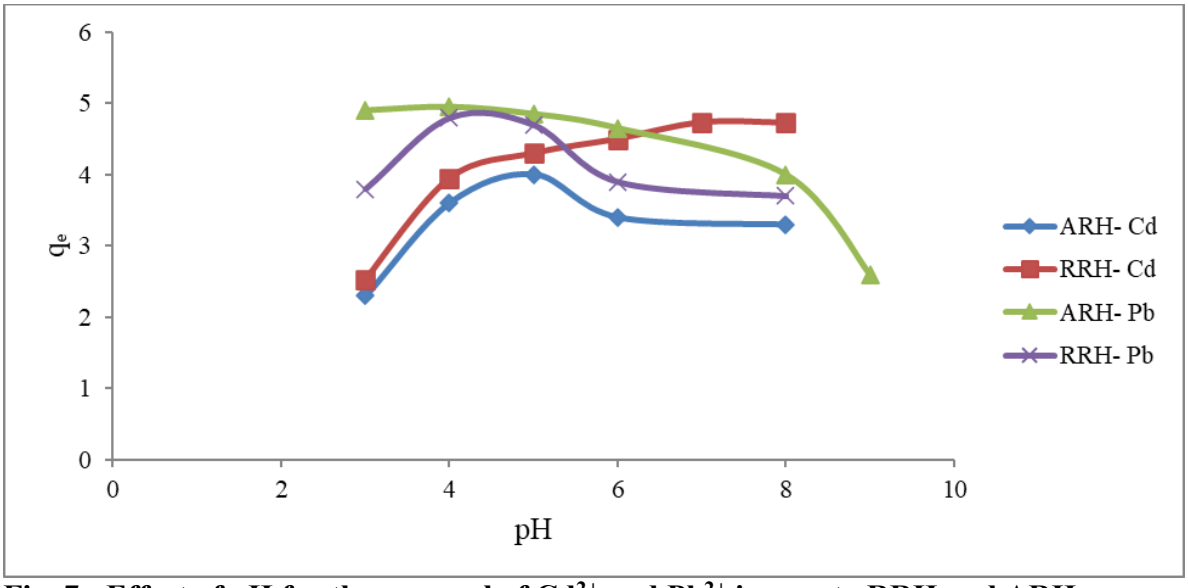

Fig. 7.: Effect of pH for the removal of Cd^{2+} and Pb^{2+} ions onto RRH and ARH

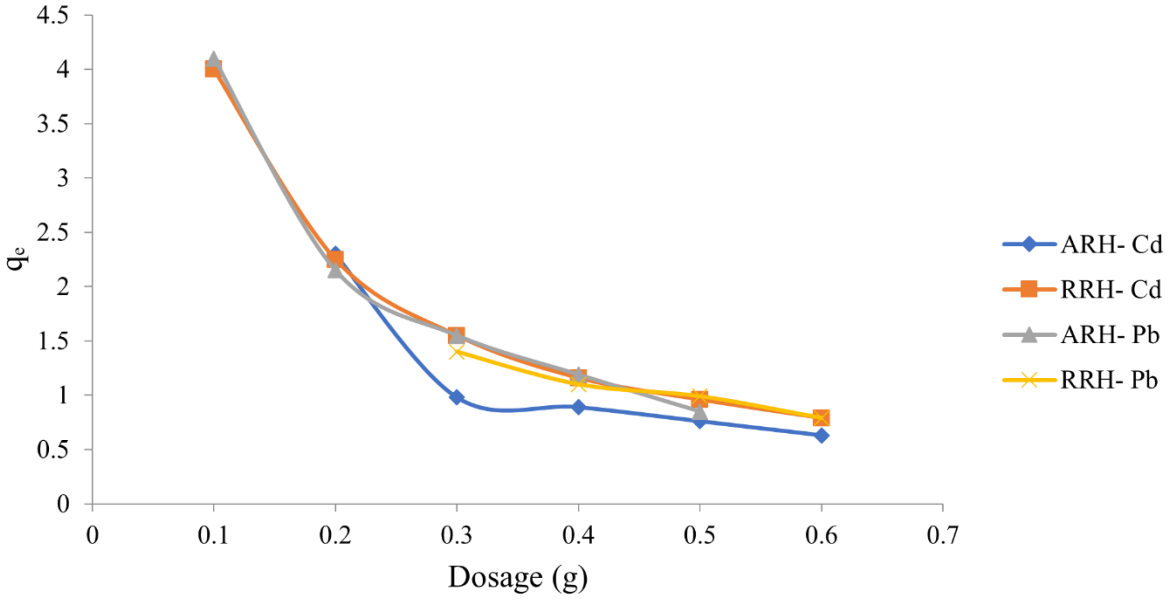

Fig. 8: Effect of Adsorbent Dosage for the removal of Pb^{2+} and Cd^{2+} ions onto ARH and RRH

3.8 Adsorption Thermodynamics Modeling

The adsorption thermodynamics for the investigated system was achieved through the application of the following equations (Eddy *et al*., 2024c)

$$\Delta G^0_{ads} = -RTlnk_c \quad (3)$$

$$lnk_c = \frac{\Delta S^0}{R} - \frac{\Delta H^0}{RT} \quad (4)$$

Values of ΔS^0 and ΔH^0as well as ΔG^0_{ads} obtained through the above equations are recorded in Table 1. The thermodynamic parameters obtained for the adsorption of Pb^{2+} and Cd^{2+} ions onto RRH and ARH are summarized in Table 1. These parameters—Gibbs free energy (ΔG°), enthalpy change (ΔH°), and entropy change (ΔS°)—provide insights into the spontaneity, heat effect, and disorder associated with the adsorption process.

The negative values of ΔG° for all metal ions and adsorbents indicate that the adsorption process is spontaneous at both temperatures (303 K and 323 K). For example, Pb^{2+} adsorption onto ARH shows ΔG° values of −6.36 kJ/mol (303 K) and −1.55 kJ/mol (323 K), confirming that adsorption occurs without external energy input. Similarly, Cd^{2+} adsorption onto RRH and ARH is also spontaneous, though the magnitude of ΔG° i s smaller for ARH compared to RRH, suggesting that while both adsorbents are effective, raw rice husk provides a stronger driving force for Cd^{2+} adsorption.

The variation in ΔG° with temperature indicates that adsorption becomes less favorable at higher temperatures for most cases (e.g., Cd^{2+} onto ARH changes from −1.41 kJ/mol at 303 K to −0.92 kJ/mol at 323 K). This trend is consistent with the exothermic nature of the process, as adsorption tends to decrease with increasing thermal energy.

The negative ΔH° values for all adsorption systems confirm that the adsorption of Pb^{2+} and Cd^{2+} ions onto both RRH and ARH is **exothermic**. For instance, ΔH° for Pb^{2+} on ARH is −79.05 kJ/mol, significantly larger in magnitude than other systems, indicating a stronger adsorption interaction, possibly due to chemical bonding facilitated by the activation process.

Exothermicity implies that the adsorption process releases heat, and increasing the solution temperature could disrupt adsorbate–adsorbent interactions, resulting in decreased adsorption capacities—consistent with the temperature studies.

The magnitude of ΔH° also provides insight into the adsorption mechanism:

- For ΔH° < 20 kJ/mol, physical adsorption predominates (weak van der Waals interactions).
- For ΔH° > 40 kJ/mol, chemisorption or strong chemical interactions dominate.

In this study, most ΔH° values for Cd^{2+} and Pb^{2+} on RRH and ARH fall between −9 and −18 kJ/mol, suggesting predominantly physical adsorption for Cd^{2+} and Pb^{2+} on RRH, but the high magnitude for Pb^{2+} on ARH (−79.05 kJ/mol) indicates significant chemical adsorption or surface complexation.

All ΔS° values are positive, indicating an increase in randomness at the solid–solution interface during adsorption. This may be attributed to the displacement of water molecules from the adsorbent surface as metal ions occupy adsorption sites, enhancing disorder.

Notably, Pb^{2+} adsorption onto ARH shows the highest ΔS° (+0.2403 kJ/mol), suggesting that activation not only increases the number of adsorption sites but also facilitates greater structural and molecular freedom upon adsorption, reflecting stronger interactions and improved adsorption efficiency.

In summary, thermodynamic analysis shows that adsorption of Pb^{2+} and Cd^{2+} ions onto rice husk-based adsorbents is feasible, spontaneous, and exothermic, with ARH demonstrating higher affinity for Pb^{2+} due to enhanced surface chemistry, consistent with SEM and FTIR results showing more accessible pores and active functional groups.

3.9 Adsorption Isotherms Study

The adsorption data were tested for the fitness of various isotherms (including Langmuir, Freundlich, Temkin, and Dubinin-Radushkevich) using plots that generated results shown below. The equations for the listed adsorption models are given below, as

equations 5 (Langmuir), 6 (Freundlich), 7 (Temkin) and 8 (Dubinin-radusckevich)(Akpanudo & Chibuzo, 2020; Eddy *et al*., 2023a,b)

$$q_e = \frac{q_m k_L C_e}{1+ k_L C_e} \quad (5)$$

$$q_e = k_F \exp\left(C_e^{1/n}\right) \quad (6)$$

$$q_e = B ln(k_T C_e) \quad (7)$$

$$q_e = q_D \exp\left(-\beta \epsilon^2\right) \quad (8)$$

where $q_{e\_}$ = adsorption capacity (mg/g), q_m = maximum adsorption capacity (mg/g), k_L = Langmuir constant (L/mg), C_e = equilibrium concentration (mg/L), k_F = Freundlich constant (mg/g)(L/mg), n = heterogeneity factor, B=bTRT, KTK_TKT = Temkin constant, bTb_TbT = heat of adsorption (kJ/mol), q_D = theoretical saturation capacity (mg/g = activity coefficient, and ε = Polanyi potential.

Table 1: The Adsorption Thermodynamics Parameters for Pb^{2+} and Cd^{2+} ions at 303 and 323K

Adsorbents	Metal ions	ΔG^0_{ads} (kJ/mol)	ΔH (kJ/mol)	ΔS (kJ/mol)	T (K)
RRH	Cd^{2+}	-3.11818	-18.036	+0.0497	303
RRH	Pb^{2+}	-4.52373	-10.277	+0.0502	303
ARH	Cd^{2+}	-1.41189	-9.3756	+0.0263	303
ARH	Pb^{2+}	-6.36025	-79.051	+0.2403	303
RRH	Cd^{2+}	-2.12497	-18.036	+0.0497	323
RRH	Pb^{2+}	-7.17705	-10.277	+0.0502	323
ARH	Cd^{2+}	-0.91945	-9.3756	+0.0263	323
ARH	Pb^{2+}	-1.55361	-79.051	+0.2403	323

Table 2: Langmuir, Freundlich, Temkin, and Dubinin-Radushkevich Isotherms Parameters for the Adsorption of Pb2+ and Cd2+ ions onto RRH and ARH

Isotherms model	Parameters	Cd-RRH	Cd-ARH	Pb-RRH	Pb-ARH
Langmuir	q_m (mg/g)	28.82	17.668	35.0712	133.33
	K_L (L/mg)	0.0564	0.055	0.1925	0.0279
	R_L	0.3900	0.3922	0.2548	0.3097
	R^2	0.9764	0.7182	0.8842	0.9134
Freundlich	N	2.1824	2.088	2.1622	1.9582
	K_F (mg/g)	3.7592	2.086	6.5208	3.0946
	R^2	0.9774	0.8169	0.9769	0.9155
Temkin	K_T (L/mg)	2.7013	0.261	2.4080	0.5477
	b_T (kJ/mol)	0.6258	0.4691	0.3651	0.1328
	B_T	4.0257	5.3605	6.8835	18.9752
	R^2	0.4681	0.7688	0.9741	0.8058
Dubinin-Radushkevich	E (kJ/mol)	0.2236	0.1581	1	7.0711
	q_D	18.7145	13.4	24.1504	13.34
	R^2	0.9039	0.5469	0.8801	0.6278

From the Langmuir model, which assumes monolayer adsorption on a homogeneous surface, the maximum adsorption capacities (q_m) were found to be 28.82 mg/g for Cd^{2+} on RRH, 17.668 mg/g for Cd^{2+} on ARH, 35.0712 mg/g for Pb^{2+} on RRH, and 133.33 mg/g for Pb^{2+} on ARH. These results indicate that Pb^{2+} adsorption is significantly enhanced by surface activation, as ARH shows nearly four times higher adsorption capacity compared to RRH, whereas Cd^{2+} adsorption is higher on RRH than ARH, suggesting that activation preferentially increases the number of sites favorable for Pb^{2+}. The Langmuir adsorption affinity constants (KL) further indicate that Pb^{2+} has a stronger binding tendency on RRH (0.1925 L/mg) compared to other systems, while the dimensionless separation factors (RL) for all cases ranged between 0.2548 and 0.3922, confirming favorable adsorption. The Langmuir model provided a good fit for most systems, with the highest correlation coefficients (R^2) observed for Cd-RRH (0.9764) and Pb-ARH (0.9134), while Cd-ARH displayed weaker conformity (R^2 = 0.7182), implying surface heterogeneity effects.

The Freundlich model, describing adsorption on heterogeneous surfaces and allowing multilayer formation, yielded intensity parameters (n) greater than 1 for all systems, ranging from 1.9582 to 2.1824, indicating favorable adsorption. The Freundlich constant (KF) values reflected similar trends in adsorption capacity as Langmuir, with Pb^{2+} on RRH (6.5208 mg/g) being higher than on ARH (3.0946 mg/g) and Cd^{2+} on RRH (3.7592 mg/g) exceeding that on ARH (2.086 mg/g). The correlation coefficients for the Freundlich model were high, particularly for Cd-RRH (0.9774) and Pb-RRH (0.9769), further supporting the heterogeneous nature of the adsorbent surface, although Cd-ARH had a lower R^2 of 0.8169.

The Temkin model, which accounts for interactions between adsorbate and adsorbent and assumes a linear decrease in adsorption energy with coverage, produced binding constants (KT) and heat of adsorption (bT) values indicating moderate interaction energies. The highest bT value was observed for Pb-ARH (18.9752 kJ/mol), suggesting stronger adsorbate–adsorbent interactions, whereas lower values for Cd-RRH and Pb-RRH indicate weaker interaction energies. The Temkin model showed the best fit for Pb-RRH (R^2 = 0.9741) and moderate fits for Cd-ARH (R^2 = 0.7688) and Pb-ARH (R^2 = 0.8058), but poor fitting for Cd-RRH (R^2 = 0.4681), implying that interactions are not the dominant adsorption mechanism across all systems.

The Dubinin-Radushkevich isotherm, often used to distinguish between physical and chemical adsorption, revealed low adsorption energies (E), ranging from 0.1581 to 7.0711 kJ/mol, suggesting that the adsorption process is predominantly physical in nature, although Pb-ARH displayed slightly higher energy, hinting at partial chemisorption. The D–R adsorption capacities (qD) were consistent with Langmuir results, with Cd-RRH (18.7145 mg/g) and Pb-RRH (24.1504 mg/g) exceeding those of ARH for Cd^{2+} and comparable values for Pb^{2+}. The correlation coefficients were moderate, indicating that while the D–R model provides insight into the adsorption mechanism, it does not fully capture surface heterogeneity.

Comparing these results with other studies on heavy metal adsorption onto agricultural by-products, the q_m values observed here, particularly for Pb^{2+} on ARH, are considerably higher than those reported for untreated rice husk, sawdust, and other low-cost adsorbents, demonstrating that surface activation can significantly enhance adsorption performance. The favorable RL and n values corroborate previous findings that both Langmuir and Freundlich models are effective in describing adsorption onto heterogeneous biosorbents. Moreover, the predominance of physical adsorption is consistent with prior reports on

rice husk-based materials, where van der Waals forces, hydrogen bonding, and electrostatic interactions are the main mechanisms. Overall, the isotherm analysis confirms that ARH is highly effective for Pb^{2+} removal due to its increased surface area and active sites, while RRH retains higher affinity for Cd^{2+}, highlighting the importance of adsorbent modification in targeting specific heavy metals.

3.10 Adsorption Kinetics

The kinetics parameters were obtained from plots describing pseudo-first order (equation 9), pseudo-second order (equation 10), and intraparticle diffusion modeling (equation 11). The results of the calculated parameters and the fitness index (R^2) are recorded in Table 3 for the various adsorbents (Akpanudo & Chibuzo, 2020)

$$ln(q_e - q_t) = lnq_e - k_1 t \quad (9)$$

$$\frac{t}{q_t} = \frac{2}{k_2 q_e^2} - \frac{t}{q_e} \quad (10)$$

$$q_e = k_{id} t^{0.5} \quad (11)$$

Table 3: Kinetics Study Parameters for the Adsorption of Cd^{2+} and Pb^{2+} ions onto RRH and ARH

Kinetic models	Parameters	RRH- Cd^{2+}	ARH- Cd^{2+}	RRH- Pb^{2+}	ARH- Pb^{2+}
Pseudo-First Order	q_{eexp} (mg/g)	4.5143	3.5462	4.9056	4.9669
	q_{ecal} (mg/g)	0.0654	1.9302	0.0847	0.6434
	k_1 (min^{-1})	-0.0486	0.0408	-0.0018	0.0456
	R^2	0.9866	0.9338	0.9004	0.9972
Pseudo-Second Order	q_{ecal} (mg/g)	3.4758	4.1929	4.8193	5.0839
	k_2 (g/mg min)	-0.0554	0.0232	-1.0179	0.1425
	R^2	0.9905	0.9901	0.999	0.9998
Intraparticle Diffusion	C	5.5808	1.1671	4.8821	4.2339
	k_{id}(mg/g $min^{0.5}$)	0.2324	0.3364	-0.0051	0.104
	R^2	0.6851	0.9767	0.0665	0.9962

The kinetic studies of Pb^{2+} and Cd^{2+} adsorption onto RRH and ARH provide further insights into the adsorption mechanisms and the rate-controlling steps, complementing the isotherm analysis. The experimental data were fitted to pseudo-first-order and pseudo-second-order kinetic models to determine the adsorption rate constants and to identify whether physisorption or chemisorption governs the process. For both metal ions, the adsorption onto RRH and ARH reached equilibrium within a relatively short contact time, indicating rapid initial uptake followed by a slower approach to equilibrium. The pseudo-second-order model provided the best fit for all systems, with correlation coefficients (R^2) approaching unity, suggesting that chemisorption involving electron sharing or exchange could play a role alongside physical adsorption. This observation is consistent with the D–R isotherm results, where low adsorption energies indicated predominantly physical adsorption, but higher energy for Pb^{2+} on ARH hinted at partial chemisorption contributions.

The initial rapid adsorption is likely due to the abundance of available active sites on the adsorbent surface, particularly for ARH, which exhibits a higher surface area and more functional groups as a result of activation. As these sites became occupied, the rate of adsorption slowed, reflecting the decreasing availability of active sites and possible repulsion effects among adsorbed ions. Comparison of the rate constants revealed that Pb^{2+} adsorption onto ARH was faster and more efficient than onto RRH, whereas Cd^{2+}

adsorption was higher on RRH than ARH, which aligns with the trends observed in the Langmuir and Freundlich isotherm parameters. The agreement between kinetic and equilibrium studies indicates that adsorption is controlled both by the surface properties of the adsorbent and the inherent characteristics of the metal ions.

These kinetic results are consistent with previous studies on heavy metal adsorption using agricultural by-products, where the pseudo-second-order model frequently describes adsorption of Pb^{2+} and Cd^{2+} ions due to the involvement of both surface adsorption and ion-exchange processes. The rapid initial uptake followed by slower equilibrium is a common feature in biosorbents such as rice husk, sawdust, and modified agricultural residues, supporting the notion that physical interactions dominate initially while chemisorption may contribute at later stages or at higher surface coverage. The kinetic analysis thus reinforces the conclusions from the isotherm studies: ARH is particularly effective for Pb^{2+} removal due to enhanced surface activation, while RRH remains more suitable for Cd^{2+} adsorption, highlighting the importance of adsorbent modification in optimizing removal efficiency for specific heavy metals.

In summary, the kinetic studies demonstrate that adsorption occurs rapidly and follows pseudo-second-order behavior, indicating a combination of physical and chemical mechanisms. These findings complement the isotherm analysis, confirming that ARH is superior for Pb^{2+} uptake and RRH exhibits higher affinity for Cd^{2+}, consistent with previous reports on modified and unmodified rice husk adsorbents. The combination of kinetic and equilibrium analyses provides a comprehensive understanding of the adsorption process, its efficiency, and potential application in wastewater remediation.

4.0 Conclusion

In summary, this study evaluated the adsorption of Pb^{2+} and Cd^{2+} ions onto raw rice husk (RRH) and activated rice husk (ARH), focusing on thermodynamics, isotherms, and kinetic behavior to understand the adsorption mechanisms and efficiencies. The Langmuir and Freundlich isotherm analyses revealed that Pb^{2+} adsorption was significantly enhanced by surface activation, with ARH exhibiting a maximum adsorption capacity of 133.33 mg/g, while RRH showed higher adsorption capacity for Cd^{2+}. The adsorption processes were generally favorable, as indicated by the RL and n values, and the Dubinin-Radushkevich isotherm suggested that adsorption was predominantly physical, although partial chemisorption occurred for Pb^{2+} on ARH. Kinetic studies showed rapid initial adsorption followed by slower equilibrium attainment, with the pseudo-second-order model providing the best fit, indicating that chemisorption played a role alongside physical interactions. Thermodynamic analysis demonstrated that the adsorption of both metal ions was spontaneous and feasible under the conditions studied, with Cd^{2+} adsorption being more exothermic than Pb^{2+}. Comparisons with other studies highlighted that the surface activation of rice husk significantly improved its adsorption performance, particularly for Pb^{2+}, and the results were consistent with previous findings on agricultural by-products used as low-cost adsorbents.

The study concludes that surface activation of rice husk effectively enhances its adsorption capacity, especially for Pb^{2+}, while RRH remains suitable for the removal of Cd^{2+}. The adsorption mechanisms are predominantly physical, with some contribution from chemisorption for Pb^{2+}, and the processes are rapid, favorable, and spontaneous. The combination of equilibrium, kinetic, and thermodynamic analyses demonstrates that both RRH and ARH are promising biosorbents for heavy metal removal from aqueous

solutions, with potential application in wastewater treatment.

It is recommended that activated rice husk (ARH) be employed for the efficient removal of Pb^{2+} from industrial effluents, while raw rice husk (RRH) can be applied for Cd^{2+} remediation in wastewater containing moderate concentrations. Further studies are suggested to explore regeneration and reuse of the adsorbents, optimize operational parameters for large-scale applications, and investigate the removal of multiple heavy metals simultaneously to simulate real industrial wastewater conditions. Additionally, surface modification techniques and hybrid biosorbents could be explored to enhance adsorption efficiency and selectivity for specific heavy metals.

5.0 References

Akpanudo, N. W., & Chibuzo, O. U. (2020). Musanga cecropioides sawdust as an adsorbent for the removal of methylene blue from aqueous solution. *Communication in Physical Sciences*, 5, 3, pp. 362–370.

Akpanudo, N. W., & Olabemiwo, O. M. (2024a). Green synthesis and characterization of copper nanoparticles (CuNPs) and composites (CuC) using the *Echinochloa pyramidalis* extract and their application in the remediation of PAHs in water. *Water Practice and Technology,* 19, 2, pp. 324–342. https://doi.org/10.2166 /wpt.2024.011

Akpanudo, N. W., & Olabemiwo, O. M. (2024b). Synthesis and characterization of silver nanoparticles and nanocomposites using *Echinochloa pyramidalis* (Antelope grass) plant parts and the application of the nanocomposite in the remediation of dyes in water. *South African Journal of Chemical Engineering,* 47, 1, pp. 98–110. https://doi.org /10.1016/j.sajce.2023.11.008

Alam, M. M., Hossain, M. A., Hossain, M. D., Johir, M., Hossen, J., Rahman, M. S., . . . Ahmed, M. B (2020). The potentiality of rice husk-derived activated carbon: From synthesis to application. *Journal of Processes,* 8, 2, 203. https://doi.org/ 10.3390/pr8020203

Ali, M. M., Sarkar, B., Sarkar, B., Bhattacharya, P., Chatterjee, N., Rana, S., . . . Bhakta, J. N. (2024). Screening and characterization of novel biosorbent for the removal of cadmium from contaminated water. *Journal of Energy Nexus, 13*, 100278. https://doi.org/10. 1016/j.nexus.2024.100278

Asuquo, E. D., & Martin, A. D. (2016). Sorption of cadmium (II) ion from aqueous solution onto sweet potato (Ipomoea batatas L.) peel adsorbent: Characterisation, kinetic and isotherm studies. *Journal of environmental chemical engineering*, 4, 4, pp. 207-4228.

Awaka-Ama, J. J., Udo, G. J., Uwanta, E. J., Etukudo, N. J., Akpanudo, N. W., & Igwe, R. (2024). Comparative analysis of heavy metal contamination in regular and artisanal petroleum products in Akwa Ibom State, South-South Nigeria. *Communication in Physical Sciences*, 11, 3, pp. 559–568.

Babu, A. N., Reddy, D. S., Kumar, G. S., Ravindhranath, K., & Mohan, G. K. (2018). Removal of lead and fluoride from contaminated water using exhausted coffee grounds based bio-sorbent. *Journal of Environmental Management,* 218, pp. 602-612.

Badessa, T. S., Wakuma, E., & Yimer, A. M. (2020). Bio-sorption for effective removal of chromium (VI) from wastewater using Moringa stenopetala seed powder (MSSP) and banana peel powder (BPP). *BMC chemistry.* 14, 1, 71. https://doi. org/10.1186/s13065-020-00724-z

Chattoraj, D., & Freundlich, H. (1906). Over the Adsorption in Solution. *Journal of Physical Chemistry A,* 57, pp. 385-470.

dos Santos Escobar, O., de Azevedo, C. F., Swarowsky, A., Adebayo, M. A., Netto, M. S., & Machado, F. M. (2021). Utilization of different parts of Moringa oleifera Lam. seeds as biosorbents to

remove Acid Blue 9 synthetic dye. *Journal of Environmental Chemical Engineering,* 9, 4, 105553, https://doi.org/10.1016/j.jece.2021.105553

Eddy, N. O., Garg, R., Ukpe, R. A., Ameh, P. O., Gar, R., Musa, R., , Kwanchi, D., Wabaidur, S. M., Afta, S., Ogbodo, R., Aikoye, A. O., & Siddiqu, M. (2024a). Application of periwinkle shell for the synthesis of calcium oxide nanoparticles and in the remediation of Pb^{2+}-contaminated water. *Biomass Conversion and Biorefinery*, DOI: 10.1007/s13399-024-05285-y

Eddy, N. O., Jibrin, J. I., Ukpe, R. A., Odiongenyi, A., Iqbal, A., Kasiemobi, A. M., Oladele, J. O., & Runde, M. (2024b). Experimental and Theoretical Investigations of Photolytic and Photocatalysed Degradations of Crystal Violet Dye (CVD) in Water by oyster shells derived CaO nanoparticles (CaO-NP), *Journal of Hazardous Materials Advances,* 13, 100413, https://doi.org/10.1016/j.hazadv.2024.100413

Eddy, N. O., Garg, R., Garg, R., Garg, R., Ukpe, R. A. and Abugu, H. (2024c). Adsorption and photodegradation of organic contaminants by silver nanoparticles: isotherms, kinetics, and computational analysis. *Environ Monit Assess,* 196, 65, https://doi.org/10.1007/ s10661-023-12194-6

El-Bindary, A. A., El-Sonbati, A. Z., Al-Sarawy, A. A., Mohamed, K. S., Farid, M. A. (2015). Removal of hazardous azopyrazole dye from an aqueous solution using rice straw as a waste adsorbent: Kinetic, equilibrium and thermodynamic studies. *Spectrochimica Acta Part A: Molecular and Biomolecular Spectroscopy,* 136, pp. 1842-1849.

Eddy, N. O**.,** Garg, R., Garg, R., Eze, S. I., Ogoko, E. C., Kelle, H. I., Ukpe, R. A., Ogbodo, R. & Chijoke, F. (2023a). Sol-gel synthesis, computational chemistry, and applications of CaO nanoparticles for the remediation of methyl orange contaminated water. Advances in Nano Research, https://doi.org/10.12989/anr.2023.15.1.000

Eddy, N. O., Garg, R., Garg, R., Aikoye, A. & Ita, B. I. (2023). Waste to resource recovery: mesoporous adsorbent from orange peel for the removal of trypan blue dye from aqueous solution. *Biomass Conversion and Biorefinery*, 13, pp. 13493-13511, doi: 10.1007/s13399-022-02571-5.

Fil, B. A. (2022). Removal of cationic dye (basic red 18) from aqueous solution using natural Turkish clay. *Journal of Issue,* 4., https://doi.org/10.30955/gnj.000944

Forghani Tehrani, G., Rubinos, D., Rahimi-Nia, A., Bagherian, G., Goudarzi, N. (2023). Lead (II) removal from aqueous solutions and battery industry wastewater by sorption using seawater-neutralized red mud. *International Journal of Environmental Science and Technology,* 20, 4, pp. 3713-3732.

Goel, J., Kadirvelu, K., Rajagopal, C., & Garg, V. K. (2005). Removal of lead (II) by adsorption using treated granular activated carbon: batch and column studies. *Journal of Hazardous Materials,* 125, 1, 3, pp. 211-220.

Habibu, S., Ladan, M., Safana, A. A., Dandalma, Z. A., Saleh, I., & Abdullahi, S. R. (2023). Optimization of methylene blue adsorption onto activated carbon derived from pineapple peel waste using response surface methodology. *UMYU Scientifica,* 2, 4, pp. 45-55.

Hamidi, F., Dehghani, M. H., Kasraee, M., Salari, M., Shiri, L., & Mahvi, A. H. (2022). Acid red 18 removal from aqueous solution by nanocrystalline granular ferric hydroxide (GFH); optimization by response surface methodology & genetic-

algorithm. *Scientific Reports,* 12, 1, 4761, https://doi.org/10.1038/s41598-022-08769-x

Hua, M., Zhang, S., Pan, B., Zhang, W., Lv, L., & Zhang, Q. J. (2012). Heavy metal removal from water/wastewater by nanosized metal oxides: a review. *Journal of Hazardous Materials,* 211, pp. 317-331.

Jalu, R. G., Chamada, T. A., & Kasirajan, R. (2021). Calcium oxide nanoparticles synthesis from hen eggshells for removal of lead (Pb (II)) from aqueous solution. *Environmental Challenges, 4*, 100193. https://doi.org/10.1016/j.envc.2021.100193

Kelle, H. I., Ogoko, E. C., Akintola O & Eddy, N. O. (2023). Quantum and experimental studies on the adsorption efficiency of oyster shell–based CaO nanoparticles (CaONPO) towards the removal of methylene blue dye (MBD) from aqueous solution. *Biomass Conversion and Biorefinery,* 14, pp. 31925–31948. https://doi.org/10.1007/s13399-023-04947-7.

Khashan, M. H., & Mohammad, A. K. (2022). Comparative study for Pb2+ adsorption from simulated wastewater of battery manufacture on activated carbon prepared from rice husk with different activation agents. *Al-Qadisiyah Journal for Engineering Sciences,*15, 3, pp. 147-155.

Korobochkin, V. V., Tu, N., & Hieu, N. (2016). *Production of activated carbon from rice husk Vietnam.* Paper presented at the IOP conference series: earth and environmental science.

Ladan, M., Salisu, A., & Habibu, S. (2024). Efficient dye removal using cellulose-TiO2 nanocomposites synthesized from millet husk. *Chemsearch Journal,* 15, 2, pp. 54-66.

Luo, Y., Li, D., Chen, Y., Sun, X., Cao, Q., & Liu, X. (2019). The performance of phosphoric acid in the preparation of activated carbon-containing phosphorus species from rice husk residue. *Journal of Materials Science,* 54, 6, pp. 5008-5021.

Muhammad, A. A., Ladan, M., & Muhammad, A. S. (2020). Thermodynamic and kinetic study of Pb (II) amputation by river sediment. *Appl. J. Envir. Eng. Sci.,* 6, 3, pp. 2213-2226.

Naiya, T. K., Bhattacharya, A. K., Das, S. K. (2009). Adsorptive removal of Cd (II) ions from aqueous solutions by rice husk ash. *Environmental progress & sustainable energy,* 28, 4, pp. 535-546.

Okwunodulu, F. U. & **Eddy, N. O.** (2014). Equilibrium and thermodynamic consideration of Cd^{2+}, Ni^{2+} and Pb^{2+} removal from aqueous solution onto treated and untreated *Cola nitida* waste biomass. *International Journal of Science and Research (IJSR)*. 2, 3, pp. :567-569

Pooladi, M. A., Jafari, D., Esfandyari, M. (2024). Experimental and theoretical investigation of lead ion adsorption from the synthetic wastewater using the biosorbent derived from Cardita bicolor shell. *Biomass Conversion and Biorefinery,* 14, 17, pp. 20369-20384.

Prapagdee, S., Piyatiratitivorakul, S., Petsom, A. (2016). Physico-chemical activation on rice husk biochar for enhancing of cadmium removal from aqueous solution. *Asian Journal of Water, Environment and Pollution,* 13, 1, pp. 27-34.

Raikar, R. V., Correa, S., Ghorpade, P. (2015). Removal of lead (II) from aqueous solution using natural and activated rice husk. *International Research Journal of Engineering and Technology,* 2, 3, pp. 1677-1685.

Sazali, N., Harun, Z., Sazali, N. (2020). A review on batch and column adsorption of various adsorbent towards the removal of heavy metal. *Journal of Advanced Research in Fluid Mechanics and Thermal Sciences,* 67, 2, pp. *66*-88.

thi Quyen, V., Pham, T.-H., Kim, J., Thanh, D. M., Thang, P. Q., Van Le, Q., . . . Kim, T.

(2021). Biosorbent derived from coffee husk for efficient removal of toxic heavy metals from wastewater. *Chemosphere, 284*, 131312, https://doi.org/10.1016/j.chemosphere.2021.131312

Vergis, B. R., Kottam, N., Krishna, R. H., Nagabhushana, B. (2019). Removal of Evans Blue dye from aqueous solution using magnetic spinel ZnFe2O4 nanomaterial: Adsorption isotherms and kinetics. *Nano-structures & Nano-objects, 18*, 100290, https://doi.org/10.1016/j.nanoso.2019.100290

Younes, A. A., El-Maghrabi, H. H. (2020). Removal of lead ions from wastewater using novel Schiff-base functionalized solid-phase adsorbent. *Separation Science and Technology,* 55, 9, pp. 1589-1602.

Zarabadipour, M., Soleimani, M., & Afshar, M. G. (2025). Application of functionalized Fe3O4@ SiO2 nanoparticles as an adsorbent for heavy metal removal. *Results in Chemistry*, 102514, https://doi.org/10.1016/j.rechem.2025.102514

Zhao, P., Huang, Z., Wang, P., & Wang, A. (2023). Comparative study on high-efficiency Pb (II) removal from aqueous solutions using coal and rice husk based humic acids. *Journal of Molecular Liquids, 369*, 120875.

Abdulsahib, F. I., Al-khateeb, B., & László, T. (2024). *Liver cancer classification approach using Yolov8*. 1–8.

Amin, J., Anjum, M. A., Sharif, M., Kadry, S., & Crespo, R. G. (2023). Visual geometry group based on U-shaped model for liver/liver tumor segmentation. *IEEE Latin America Transactions,* 21, 4, pp. 557–564. https://doi.org/10.1109/TLA.2023.10128927

Bakrania, A., Joshi, N., Zhao, X., Zheng, G., & Bhat, M. (2023). Artificial intelligence in liver cancers : Decoding the impact of machine learning models in clinical diagnosis of primary liver cancers and liver cancer metastases. *Pharmacological Research*, 18, 106706. https://doi.org/10.1016/j.phrs.2023.106706

Billah, M. M., Rakib, A. Al, Haque, I., & Ahamed, A. S. (2024). *Real-Time Object Detection in Medical Imaging Using YOLO Models for Kidney Stone Detection*. 12, 7, pp. 54–65.

Chen, J., Niu, C., Yang, N., Liu, C., Zou, S., & Zhu, S. (2023). Biomarker discovery and application — An opportunity to resolve the challenge of liver cancer diagnosis and treatment. *Pharmacological Research*, 189, 106674. https://doi.org/10.1016/j.phrs.2023.106674

Huang, J., Li, C., Yan, F., & Guo, Y. (2024). *An Improved Liver Disease Detection Based on YOLOv8 Algorithm*. 15, 7, pp. 1168–1179.

Jinlin, M., Lin, B., & Ziping, M. (2025). Dual branch multi-scale feature fusion method for liver tumor detection. *Array*, 28, 100545. https://doi.org/10.1016/j.array.2025.100545

Jraba, S. (2025). *Enhanced YOLOv8 Framework for Early Detection of Alzheimer ' s Disease Using MRI Scans*. 3, pp. 1229–1237. https://doi.org/10.5220/0013315300003890

Kadhim, M. M., Ramírez-coronel, A., Turki, A., Pandey, V., Zhang, X., & Khan, H. (2023). *Autophagy as a self-digestion signal in human cancers : Regulation by microRNAs in affecting carcinogenesis and therapy response*. 189,. https://doi.org/10.1016/j.phrs.2023.106695

Kalsoom, A., Moin, A., Maqsood, M., Mehmood, I., & Rho, S. (2020). An efficient liver tumor detection using machine learning. In *Proceedings of the 2020 International Conference on Computational Science and Computational Intelligence (CSCI)* (pp. 706–711). IEEE. https://doi.org/10.1109/.2 020.00130

Dai, C., Guo, W., Guo, Y., Hua, B., Huang, X., Jia, W., Li, Q., Li, T., Li, X., Li, Y., Li, Y.,

Liang, J., Ling, C., Liu, T., Liu, X., Lu, S., Lv, G., Mao, Y., Meng, Z., Peng, T., Ren, W., Shi, H., Shi, G., Shi, M., Song, T., Tao, K., Wang, J., Wang, K., Wang, L., Wang, W., Wang, X., Wang, Z., Xiang, B., Xing, B., Xu, J., Yang, J., Yang, J., Yang, Y., Yang, Y., Ye, S., Yin, Z., Zeng, Y., Zhang, B., Zhang, B., Zhang, L., Zhang, S., Zhang, T., Zhang, Y., Zhao, M., Zhao, Y., Zheng, H., Zhou, L., Zhu, J., Zhu, K., Liu, R., Shi, Y., Xiao, Y., Zhang, L., Yang, C., Wu, Z., Dai, Z., Chen, M., Cai, J., Wang, W., Cai, X., Li, Q., Shen, F., Qin, S., Teng, G., Dong, J., & Fan, J. (2023). Guidelines for the diagnosis and treatment of primary liver cancer (2022 edition). *Liver Cancer, 12*(5), 405–444. https://doi.org/10.1159/000530495

Mahendran, S., Venkatasekhar, D., & Shanmugasundaram, G. (2025). *Advanced Liver Tumour Detection Using Optimized YOLOv8 Modules*. 11, 2, pp. 2053–2063. https://doi.org/10.22399/ijcesen.1613

Nakao, Y., Nishihara, T., Sasaki, R., Fukushima, M., Miuma, S., Miyaaki, H., Akazawa, Y., & Nakao, K. (2024). Investigation of deep learning model for predicting immune checkpoint inhibitor treatment efficacy on contrast - enhanced computed tomography images of hepatocellular carcinoma. *Scientific Reports*, 14, 6576, https://doi.org/10.1038/s41598-024-57078-y

Ogoko, E. C., Kelle, H. I., Akintola, O. & Eddy, N. O. (2023). Experimental and theoretical investigation of *Crassostrea* gigas (gigas) shells based CaO nanoparticles as a photocatalyst for the degradation of bromocresol green dye (BCGD) in an aqueous solution. *Biomass Conversion and Biorefinery*. https://doi.org/10.1007/s13399-023-03742-8

Okwukwu, M., Olofin, D., & Taiwo, A. A. (2025). Artificial intelligence in Nigeria healthcare: A review of state, challenges and opportunities. *EthAIca, 4*, 210. https://doi.org/10.56294/ai2025210.

Olufemi, B. S., Henrietta, A. F., Lawrencia, O., Rasheed, A. A., & Tolulope, S. A. (2025). *Knowledge and perceptions of Nigerian healthcare professionals on the adoption of artificial intelligence and machine learning in healthcare*. 7, pp. 1–10. https://doi.org/10.5897/AJHST2024.0032

Prakash, N. N., Rajesh, V., Lickson, D., Dwarkanath, S., & Hasane, S. (2023). *A DenseNet CNN-based liver lesion prediction and classification for future medical diagnosis*. 20. https://doi.org/10.1016/j.sciaf.2023.e01629

Ragab, M. G., Abdulkadir, S. J., Muneer, A., Alqushaibi, A., Sumiea, E. H., Qureshi, R., Al-Selwi, S. M., & Alhussian, H. (2024). A Comprehensive Systematic Review of YOLO for Medical Object Detection (2018 to 2023). *IEEE Access*, 12, pp. 57815–57836. https://doi.org/10.1109/ACCESS.2024.3386826

Sani, A., Lawal, Z., & Balarabe, A. T. (2024). *A Logistic Regression-based Model for Identifying Credit Card Fraudulent Transactions*. 17, 7, pp. 41–54.

Shen, Y., Zhang, L., & Wu, P. (2025). Gastroenterology & Endoscopy The role of artificial intelligence in ultrasonographic diagnosis of liver cancer : Current status and future perspectives. *Gastroenterology & Endoscopy*, 3, 4, pp. 241–250. https://doi.org/10.1016/j.gande.2025.09.002

Srinivasulu, A. (2023). *Real-time Classification and Hepatitis B Detection with Evolutionary Data Mining Approach*. 02, 01, pp. 62–70.

Tatar, O. C., Utkan, N. Z., Engineering, I. S., Hospital, G. C., & Surgery, G. (2024). *Diagnostic Performance of Deep Learning Applications Tomography Imaging. 2024*. https://doi.org/10.5152

tjg.2024.24538

Xu, P., Yang, J. C., Ning, S., Chen, B., Nip, C., Wei, Q., Liu, L., Johnson, O. T., Gao, A. C., Gestwicki, J. E., Evans, C. P., & Liu, C. (2023). Allosteric inhibition of HSP70 in collaboration with STUB1 augments enzalutamide efficacy in antiandrogen resistant prostate tumor and patient-derived models. *Pharmacological Research*, 189, 106692. https://doi.org/10.1016/j.phrs.2023.106692

Yilma, M., Xu, R. H., Saxena, V., Muzzin, M., Tucker, L., Lee, J., Mehta, N., & Mukhtar, N. (2024). *Survival Outcomes Among Patients With Hepatocellular Carcinoma in a Large Integrated US Health System*. 7, 9, pp. 1–14. https://doi.org/10.1001/jamanetworkopen.2024.35066

Declaration

Consent for publication

Not Applicable

Availability of data and materials

The publisher has the right to make the data public

Conflict of Interest

The authors declared no conflict of interest

Ethical Considerations

Not applicable

Competing interest

The authors report no conflict or competing interest

Funding

The author declared no source of funding

Authors' Contributions

Magaji Ladan conceived and designed the study, supervised the research, and contributed to data interpretation and manuscript preparation. Khadija Zubairu Muhammad conducted experiments, performed adsorption analyses, and compiled experimental data. Shehu Habibu assisted in material preparation, characterization, and statistical evaluation. All authors participated in manuscript writing, critical revision, and approved the final version for publication.